Reaction-based fluorescent sensor for investigating mobile Zn[superscript 2+] in mitochondria of healthy versus cancerous prostate cells

Citation: Chyan, W., D. Y. Zhang, S. J. Lippard, and R. J. Radford. "Reaction-Based Fluorescent Sensor for Investigating Mobile Zn[superscript 2+] in Mitochondria of Healthy Versus Cancerous Prostate Cells." Proceedings of the National Academy of Sciences 111, no. 1 (December 12, 2013): 143–148.

As Published: http://dx.doi.org/10.1073/pnas.1310583110

Publisher: National Academy of Sciences (U.S.)

Persistent URL: http://hdl.handle.net/1721.1/89120

Version: Final published version: final published article, as it appeared in a journal, conference proceedings, or other formally published context

Reaction-based fluorescent sensor for investigating mobile Zn^{2+} in mitochondria of healthy versus cancerous prostate cells

Wen Chyan, Daniel Y. Zhang, Stephen J. Lippard[1], and Robert J. Radford[1]

Department of Chemistry, Massachusetts Institute of Technology, Cambridge, MA 02139

Edited by Harry B. Gray, California Institute of Technology, Pasadena, CA, and approved November 13, 2013 (received for review June 3, 2013)

Chelatable, mobile forms of divalent zinc, Zn(II), play essential signaling roles in mammalian biology. A complex network of zinc import and transport proteins has evolved to control zinc concentration and distribution on a subcellular level. Understanding the action of mobile zinc requires tools that can detect changes in Zn(II) concentrations at discrete cellular locales. We present here a zinc-responsive, reaction-based, targetable probe based on the diacetyled form of Zinpyr-1. The compound, (6-amidoethyl)triphenylphosphonium Zinpyr-1 diacetate (DA-ZP1-TPP), is essentially nonfluorescent in the metal-free state; however, exposure to Zn (II) triggers metal-mediated hydrolysis of the acetyl groups to afford a large, rapid, and zinc-induced fluorescence response. DA-ZP1-TPP is insensitive to intracellular esterases over a 2-h period and is impervious to proton-induced turn-on. A TPP unit is appended for targeting mitochondria, as demonstrated by live cell fluorescence imaging studies. The practical utility of DA-ZP1-TPP is demonstrated by experiments revealing that, in contrast to healthy epithelial prostate cells, tumorigenic cells are unable to accumulate mobile zinc within their mitochondria.

reaction-based probe | prostate cancer | zinc biology | fluorescence microscopy

Divalent zinc, Zn(II), is a trace nutrient critical for physiological function. Although most biological zinc ions are tightly associated with proteins (1), pools of loosely bound or "mobile" forms (2) serve regulatory or signaling functions (3), including nucleation of protein self-assembly (4), triggering of signaling pathways (5), and modification of cellular metabolism (6). In this capacity, mobile zinc performs essential tasks in the physiology of the central nervous system, pancreas, and prostate (5, 7, 8).

Mobile zinc is an indispensable component of prostate physiology. The prostate contains more zinc than any other soft tissue in the body, and there is a clear correlation between total prostatic zinc levels and cancer (8). Despite extensive investigation, however, our molecular understanding of mobile zinc in the prostate remains incomplete (7, 8). This situation is related in part to the complex spatiotemporal mechanisms through which the prostate controls zinc levels. At least three Zrt/Irt-like proteins (ZIPs) and six zinc transport proteins (ZnT) are expressed in a lobe-dependent manner in the prostate (7); for example, the epithelium of the human peripheral lobe accumulates high concentrations of zinc, primarily through a ZIP1-dependent process (9). Inside prostate epithelial cells, Zn(II) accumulates in mitochondria, where it can inhibit aconitase and truncate the citric acid cycle, facilitating cellular buildup of citrate ion (6, 10). Alterations to prostatic zinc trafficking are incontrovertibly linked to the onset and progression of prostate cancer (11–13).

Understanding the transport, accumulation, and action of mobile zinc in the prostate and other tissues requires tools that can report on changes in mobile zinc concentration at defined locales within a live cell environment. Zinc-responsive fluorescent reporters are well suited for this purpose. Of the various classes of zinc sensors (14), small molecule fluorescein-based scaffolds are the most broadly implemented (3, 15). Fluorescein is bright ($\varepsilon\Phi$), nontoxic, and compatible with one- and two-photon microscopy (16). Fluorescein has well-established synthetic pathways and has been fashioned into probes with varying mobile zinc affinities and dynamic ranges (16). A persistent limitation of fluorescein-based sensors is their unpredictability with respect to plasma membrane permeability and subcellular localization. Seemingly small changes in chemical structure can have dramatic effects on sensor permeability and localization (15).

The capricious localization of fluorescein-based probes contrasts with protein-based zinc sensors, which offer programmable probe localization (17, 18). Although protein-based (19) and peptide-based (20) targeting strategies have recently been used to direct the localization of fluorescein-based zinc sensors, controlling the subcellular accumulation of such probes remains a significant challenge.

To avoid the unpredictability of de novo sensor design, we adopted the aminoethyltriphenylphosphonium (TPP) ion as a small chemical tag to direct a mobile zinc sensor to the mitochondrion, a well-established strategy (21–27) based on known intracellular physiochemical properties. We created a derivative of the widely applied zinc sensor ZP1 (16) with the TPP ion attached via an amide linkage to the 6-position on the benzoic acid ring of the fluorophore (Fig. 1). Unexpectedly, the resulting construct, ZP1-TPP, sequestered within endosomes/lysosomes and lost its ability to respond to changes in mobile zinc concentrations (*vide infra*).

To prevent such endosomal localization and afford TPP-mediated mitochondrial targeting in live cells, we altered the physical properties of ZP1-TPP through conversion to the fluorescein diacetate

Significance

Mobile zinc plays important roles in mammalian physiology. Understanding the action of mobile zinc requires tools to follow it within and between live cells. Zinc-selective fluorescent probes offer a facile means for detecting such mobile zinc, but small molecules constructed to perform this task typically have an unpredictable cellular distribution. Subtle changes in chemical structure can radically alter subcellular localization. To overcome this challenge, we installed a chemical unit to direct the sensor specifically to mitochondria and discovered that tumorigenic cells lose their ability to accumulate mobile zinc within these organelles. To carry out this work, we devised a reaction-based sensor that undergoes zinc-mediated chemistry, converting a nonfluorescent molecule into one that emits brightly and avoiding undesired sequestration in endo/lysosome.

Author contributions: S.J.L. and R.J.R. designed research; W.C., D.Y.Z., and R.J.R. performed research; W.C., D.Y.Z., S.J.L., and R.J.R. analyzed data; and W.C., S.J.L., and R.J.R. wrote the paper.

The authors declare no conflicts of interest.

This article is a PNAS Direct Submission.

[1]To whom correspondence may be addressed. E-mail: lippard@mit.edu or rradford@mit.edu.

This article contains supporting information online at www.pnas.org/lookup/suppl/doi:10.1073/pnas.1310583110/-/DCSupplemental.

BIOCHEMISTRY

analog. Not only did this conversion result in the desired loss of endosomal/lysosomal entrapment, but the resulting probe, (6-amidoethyl)triphenylphosphonium Zinpyr-1 diacetate (DA-ZP1-TPP), proved to have several additional highly desirable properties. The presence of the acetyl groups provided nearly complete fluorescence quenching that was rapidly reversed on exposure to Zn(II), the Lewis acidity of which mediated hydrolysis of the ester groups (28) to afford a large, rapid, zinc-induced fluorescence response (Fig. 1*B*). Moreover, DA-ZP1-TPP is insensitive to intracellular esterases over a 2-h period, impervious to proton-induced turn-on, and an excellent probe for targeting mitochondria in live cells. Unlike most reaction-based probes (29, 30), DA-ZP1-TPP also retains a measure of reversibility, owing to photo-induced electron transfer (PeT) from the dipicolylamine (DPA) groups in the apo state of the sensor (Fig. 1*C*).

To demonstrate the practical utility of DA-ZP1-TPP, we conducted live cell imaging studies of three different prostate cell lines. The results of these experiments revealed that, in contrast to healthy epithelial prostate cells, tumorigenic cells are unable to accumulate mobile zinc within their mitochondria.

Results and Discussion

ZP1-TPP is Sequestered in Endosomes/Lysosomes and Unable to Respond to Mobile Zinc. In targeting mitochondria, we relied on an aminoethyl derivative of triphenylphosphine to generate the lipophilic TPP cation (31). TPP delivers payloads, including fluorescent sensors (21–27), to the mitochondrial matrix by exploiting the negative potential maintained by actively respiring mitochondria (32). The free amino group on the aminoethyl TPP derivative provided a convenient synthetic handle for attachment of 6-CO_2H ZP1 (33). The resulting construct, ZP1-TPP, has photophysical and zinc-binding properties similar to those of other ZP1 derivatives, yielding an approximate sevenfold increased zinc-induced fluorescence response with an apparent $K_{d\text{-}Zn}$ of 0.60 (± 0.03) nM in cuvette studies (*SI Appendix*, Fig. S1). However, live cell imaging of ZP1-TPP in HeLa cells revealed a distinctive punctate pattern that did not respond significantly to changing intracellular zinc levels (Fig 2). Fluorescence imaging studies of HeLa cells pretreated with ZP1-TPP and organelle-specific dyes revealed that ZP1-TPP colocalized moderately with LysoTracker Red (Pearson's $r = 0.45 \pm 0.15$), but not at all with MitoTracker Red ($r = -0.15 \pm 0.07$) (*SI Appendix*, Fig. S2). Moreover, owing to the pH-sensitivity of ZP1 (34), when present in the acidic compartments of endosomes/lysosomes the sensor is most likely protonated, which severely diminishes the ability of ZP1-TPP to respond to mobile zinc ions (*SI Appendix*, Fig. S3).

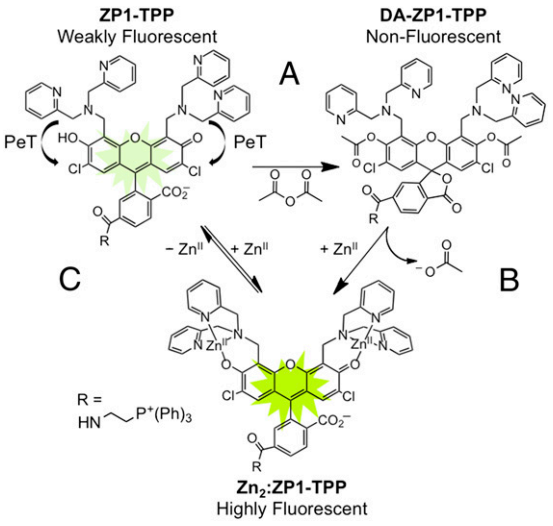

Fig. 1. Schematic representation of zinc-induced fluorescence from DA-ZP1-TPP. (*A*) ZP1-TPP is rendered nonfluorescent by addition of acetyl groups on the phenolic oxygen atoms of the xanthene ring. (*B*) Coordination of Zn(II) enhances fluorescence intensity by promoting ester hydrolysis and alleviating PeT originating from the two DPA arms. (*C*) Fluorescence enhancement is partially reversed by removing Zn(II), which restores the fluorescence-quenching ability of the DPA groups.

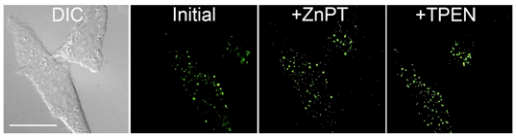

Fig. 2. Fluorescence imaging of ZP1-TPP in live HeLa cells. HeLa cells were pretreated with a 5-μM solution of ZP1-TPP in dye- and serum-free DMEM for 30 min (37 °C, 5% CO_2). Initial fluorescence images reveal a distinct punctate pattern that does not respond significantly to medium supplemented with 50 μM ZnPT or 100 μM TPEN. (Scale bar: 25 μm.)

Assessing the Physical Requirements for TPP-Mediated Targeting of Fluorophores to Mitochondria. To better understand the limitations of TPP in directing fluorophores to mitochondria, we prepared two additional TPP derivatives, one based on 6-carboxyfluorescein (FL-TPP) and the other based on coumarin 343 (C343-TPP) (*SI Appendix*, Fig. S4). We postulated that, under physiological conditions, insufficient hydrophobicity and cationic charge would prevent ZP1-TPP from accumulating in mitochondria (35, 36). At pH 7.4, ZP1-TPP [pK_a = 6.96 (34); *SI Appendix*, Fig. S5] would be a zwitterion, owing to the triphenylphosphonium ion and the 2-carboxylate anion. The negative charge of the latter would reduce TPP's effectiveness in targeting mitochondria by mitigating the positive charge on the TPP moiety and decreasing the hydrophobicity of the probe. To test this hypothesis, we conducted live cell fluorescence imaging experiments with FL-TPP. Without the appended dipicolylamine (DPA) arms, FL-TPP is predominately anionic at physiological pH [phenolic oxygen pK_a = 6.7 (37)]. Not only did FL-TPP fail to accumulate in mitochondria, it was cell-impermeable under our imaging conditions (*SI Appendix*, Fig. S6). In contrast, the cationic C343-TPP strongly colocalized with MitoTracker Red in live HeLa cells (Pearson's $r = 0.72 \pm 0.02$) (*SI Appendix*, Fig. S7).

To quantify the effect of hydrophobicity in mitochondrial targeting, we measured the octanol/aqueous buffer partition coefficient (log *P*) for our TPP constructs and two MitoTracker dyes. We then tabulated the log *P*, expected charge of the predominant species at physiological pH in solution, and cellular localization for each dye (Table 1). Based on these data, we conclude that TPP alone is insufficient to ensure mitochondrial targeting. Along with cationic charge, a minimum level of lipophilicity

Table 1. Lipophilicity, charge of predominate species in solution at physiological pH, and observed cellular localization of various dyes in live HeLa cells

Compound	log *P* value*	Charge†	Localization
MitoTracker Red	1.15 ± 0.04	+1	Mitochondria
DA-ZP1-TPP	0.74 ± 0.18	+1	Mitochondria
C343-TPP	0.72 ± 0.05	+1	Mitochondria
MitoTracker Green	0.56 ± 0.02	+1	Mitochondria
ZP1-TPP	−0.11 ± 0.01	Zwitterion	Endosome/lysosome
FL-TPP	−0.39 ± 0.03	−1	Extracellular

*Log *P* values were measured in octanol/water, buffered at pH 7 with 10 mM Tris, using a modified shake-flask procedure (*SI Appendix*).
†Charge of the predominate species in solution at pH 7.4.

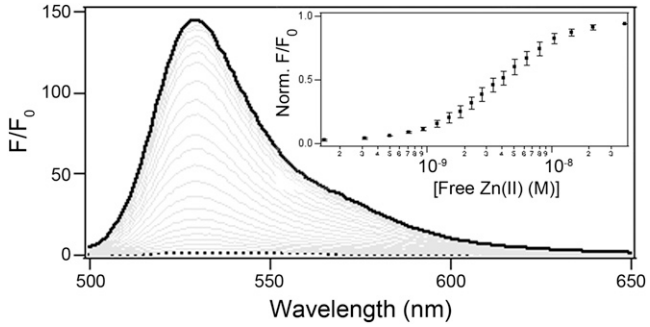

Fig. 3. Zn(II)-dependent fluorescence signal enhancement of DA-ZP1-TPP. Normalized fluorescence spectra of a 1 μM solution of DA-ZP1-TPP in buffer (50 mM PIPES, 1 mM EDTA, 2 mM $CaCl_2$, and 100 mM KCl; pH 7) on increasing concentrations of free zinc ions. (*Inset*) Zinc-binding isotherm normalized to the integrated fluorescence signal intensity under zinc-saturating conditions.

must be achieved to evade endosomal/lysosomal sequestration and enable effective mitochondrial targeting.

Design, Synthesis, and Evaluation of DA-ZP1-TPP, a Zinc Reaction-Based Probe that Targets Mitochondria. To create a ZP1-TPP derivative optimized for mitochondrial localization, we developed a reaction-based probe based on fluorescein diacetate (Scheme 1). Modifying the fluorescein scaffold with esters or ether derivatives is a common strategy to increase the cell permeability, retention, and sensitivity of fluorescein-based probes (33, 38). In traditional applications, acetyl or acetoxymethyl groups are added to the phenolic oxygen atoms of the xanthene ring structure, resulting in formation of the nonfluorescent lactone isomer (39). These modifications neutralize the negative charge from the fluorescein carboxylate, increase the overall hydrophobicity of the probe, and allow the fluorophore to readily cross the plasma membrane. Once in the cytoplasm, intracellular hydrolases typically restore the fluorescence properties of the sensors by hydrolyzing the ester functionality appended to the fluorophore (39).

Although this approach has been widely implemented (40), it relies on endogenous enzymes, the cellular expression of which can be organelle- and cell type-dependent (41). In contrast, our approach uses zinc ions to promote cleavage of the acetyl moieties, attenuate PeT quenching from the DPA arms, and restore fluorescence (Fig. 1*B*).

The diacetylated version of ZP1-TPP, designated DA-ZP1-TPP, was readily prepared by reacting ZP1-TPP with acetic anhydride overnight at room temperature. Over the course of the reaction, the mixture turned from a dark, salmon-colored solution to a light, nearly colorless liquid, which was purified by RP-HPLC. Consistent with the sensor adopting the lactone form, DA-ZP1-TPP is optically silent at $\lambda_{abs} > 350$ nm and essentially nonfluorescent ($\Phi \leq 0.001$). Adding nanomolar concentrations of free zinc ions resulted in large increases in both the absorption ($\lambda_{abs\text{-}Zn} = 510$ nm; *SI Appendix*, Fig. S8) and fluorescence ($\lambda_{em\text{-}Zn} = 529$ nm; Fig. 3) spectral bands of DA-ZP1-TPP. These optical changes combined to yield a >140-fold increase in the fluorescence signal ($\Phi_{Zn} = 0.75 \pm 0.03$; Fig. 3). Analysis of the reaction products by analytical high-pressure liquid chromatography and electrospray ionization mass spectrometry confirmed that DA-ZP1-TPP was transformed back to ZP1-TPP in the presence of Zn(II) (*SI Appendix*, Figs. S9 and S10). Whether the mode of zinc-mediated ester hydrolysis proceeds by internal or external hydroxide attack remains to be determined (42). Of note, DA-ZP1-TPP retained a measure of reversibility, differentiating it from most reaction-based probes (30). Adding a chelator (EDTA) attenuated the fluorescence signal by approximately fivefold ($\Phi = 0.15 \pm 0.02$) in the cuvette with a concomitant redshift in the absorption spectrum ($\lambda_{abs} = 522$ nm; *SI Appendix*, Fig. S8).

Reversibility of the fluorescence signal is an important feature of zinc-responsive probes, enabling confirmation that the observed increase in fluorescence signal is due to Zn(II) and not the result of an artifact. By using ZP1 as the sensor scaffold, DA-ZP1-TPP retains the quenching ability of the DPA metal-binding arms, which affords a minimally fluorescent metal-free state even after hydrolysis of the acetyl groups occurs (34). Although it cannot provide complete reversal, DA-ZP1-TPP is a rare example of a reaction-based probe with even partial reversibility (28, 30).

DA-ZP1-TPP Has a Significantly Improved pH Profile. We next investigated the pH profile of DA-ZP1-TPP. The use of nitrogen atoms to coordinate zinc endows Zinpyr sensors with selectivity for zinc over calcium and magnesium, but also renders them pH-sensitive. The pK_a values of the tertiary nitrogen atoms on the DPA units of ZP1 are 6.96 and 8.12 (34). Protonation of these amines leads to increased background fluorescence, because protons can diminish PeT in a manner similar to that of zinc ions (*SI Appendix*, Fig. S3) (34). In contrast to previous Zinpyr sensors, DA-ZP1-TPP displays no significant fluorescence turn-on under acidic conditions in the absence of zinc (Fig. 4); however, in the presence of excess zinc ions, the sensor shows a strong zinc-dependent fluorescence response at pH >5. The lack of response from DA-ZP1-TPP under acidic conditions is a significant improvement over any of the current members of the Zinpyr family. We anticipate that the use of reaction-based zinc sensors will greatly improve our ability to image mobile zinc in acidic vesicles and compartments.

DA-ZP1-TPP Yields a Zinc-Selective Fluorescence Response. DA-ZP1-TPP has a zinc-induced fluorescence response and is relatively stable to uncatalyzed hydrolysis and esterase activity. Analogous to ZP1 (43), DA-ZP1-TPP responds to Zn(II) over biologically relevant cations, such as Ca(II) and Mg(II) (Fig. 5). Other late 3d-block transition metal ions, such as Co(II) and Cu(II), can coordinate to DA-ZP1-TPP but generally are not available in appreciable chelatable quantities within the cell (44). We used UV-visible spectroscopy to investigate the rate and zinc-specificity of metal-mediated ester hydrolysis. DA-ZP1-TPP deacetylation resulted in opening of the lactone ring and restoration of conjugation across the xanthene ring, as evidenced by the change in the absorption spectrum (*SI Appendix*, Fig. S8).

By monitoring the absorbance of the xanthene π system, we could interrogate deacetylation kinetics in a manner independent of the fluorescence response. In buffer (50 mM PIPES, 100 mM KCl; pH 7) at 37 °C, adding excess $ZnCl_2$ increased the absorbance at 510 nm. The kinetic trace for this process fits well with

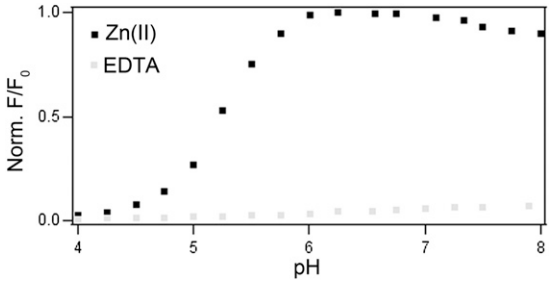

Fig. 4. Normalized fluorescence signal for DA-ZP1-TPP as a function of increasing pH in the presence of 125 μM $ZnCl_2$ (black) or 250 μM EDTA (gray). Data were acquired in 17.5 mM (0.1% vol/vol) acetic acid in Milli-Q water starting at pH 3.5. The pH of the solution was increased by sequential addition of aqueous KOH. The total volume of KOH added was less than 5% of the total volume. $\lambda_{ex} = 475$ nm.

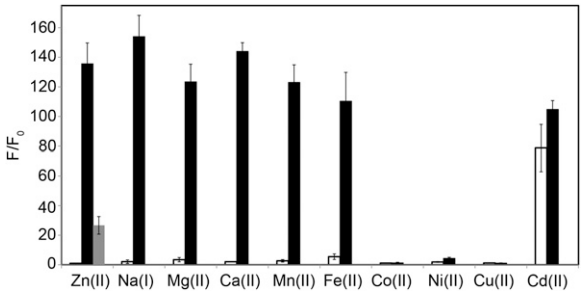

Fig. 5. Metal ion selectivity of DA-ZP1-TPP. Average normalized fluorescence intensities for a 1.1 μM solution of DA-ZP1-TPP in buffer (50 mM PIPES, 100 mM KCl; pH 7) at 25 °C, after addition of 50 μM–2 mM concentrations of various metal ions (white bars), followed by addition of 50 μM $ZnCl_2$ (black bars). The gray column represents the average sensor intensity after addition of 100 μM EDTA. Data were normalized to initial measured emission intensity.

a single exponential function with $t_{1/2\text{-Zn}}$ = 8.1 s (Fig. 6 and *SI Appendix*, Fig. S11 and Table S2). The reaction rate, as monitored by fluorescence enhancement, is independent of zinc concentration (*SI Appendix*, Table S4). This result is consistent with the fast rate (k ~10^6 M^{-1} s^{-1}, 25 °C) of zinc binding for other Zinpyr derivatives (45), implying that either ester hydrolysis or lactone ring opening is the rate-determining step (*SI Appendix*, Fig. S12). In contrast, in the presence of 250 μM EDTA or 1.25 U of porcine liver esterase, the rate of deacetylation for DA-ZP1-TPP is dramatically slower, with a $t_{1/2\text{-EDTA}}$ of 8.6 h and $t_{1/2\text{-esterase}}$ of 2.9 h (Fig. 6 and *SI Appendix*, Fig. S11 and Table S2).

Of note, both Cu(II) and Co(II) can mediate ester hydrolysis. These observations are consistent with the reported hydrolytic ability of both metal ions in small-molecule biomimetic and sensing systems (42, 46–48). Co(II)-mediated ester hydrolysis was fit to a single exponential function with $t_{1/2\text{-Co(II)}}$ = 3.04 s (*SI Appendix*, Fig. S11 and Table S2), whereas Cu(II) had significantly slower kinetics requiring two sequential irreversible steps for a good fit. The calculated half-lives for the two irreversible steps were $t_{1/2}$ = 6.08 min and $t_{1/2}$ = 39.5 min, respectively (*SI Appendix*, Fig. S11 and Table S2). As shown in Fig. 5, however, cross-reactivity with Co(II) and Cu(II) would quench the fluorescence signal and thus would not lead to any false fluorescence response.

To determine whether ester hydrolysis depends on the metal-binding core of DA-ZP1-TPP, we measured the deacetylation kinetics of fluorescein diacetate (DA-FL) under analogous conditions. As expected, DA-FL responded rapidly to esterase, but was relatively stable to hydrolysis and zinc-mediated deacetylation (*SI Appendix*, Fig. S13 and Table S3). The prolonged stability of DA-ZP1-TPP with respect to hydrolytic and enzymatic deacetylation in the absence of zinc ions, coupled with the rapid zinc-induced fluorescence response of the prosensor, indicate that DA-ZP1-TPP can serve as an effective cellular imaging agent for mobile zinc.

DA-ZP1-TPP Is Stable to Intracellular Hydrolases, Targets Mitochondria, and Responds to Changes in Intracellular Zinc Levels. We used HeLa cells as a model system to evaluate the ability of DA-ZP1-TPP to target mitochondria and respond to changes in intracellular zinc levels. Live HeLa cells were pretreated with medium containing 1 μM DA-ZP1-TPP and 250 nM MitoTracker Red for 30 min (37 °C, 5% CO_2) before imaging (Fig. 7). Initial images showed minimal fluorescence intensity from the construct (Fig. 7*B*), consistent with the low endogenous levels of mobile zinc in HeLa cells (17). Over a 2-h period, the fluorescence intensity from the sensor remained constant, implying that the acetylated form is stable against intracellular esterases (Fig. 7*F*). Adding 50 μM Zn/pyrithione (ZnPT) resulted in an ~12-fold increase in fluorescence intensity that visually overlapped with the signal from MitoTracker Red (Fig. 7 and *SI Appendix*, Figs. S14 and S15). Quantitative analysis of the fluorescence signals obtained from MitoTracker Red and zinc-bound ZP1-TPP revealed that the two dyes had good colocalization (Pearson's r = 0.64 ± 0.1). Adding 100 μM *N*,*N*,*N*′,*N*′-tetrakis(2-pyridylmethyl)ethylenediamine (TPEN) attenuated the fluorescence signal by 2.4-fold (Fig. 7*G*).

Based on these fluorescence microscopy studies with HeLa cells, we conclude that (*i*) in contrast to the nonacetylated form of the sensor (*vide supra*), DA-ZP1-TPP has sufficient cationic character and hydrophobicity (log P = 0.74 ± 0.18; Table 1) to target mitochondria effectively; (*ii*) DA-ZP1-TPP is stable against intracellular hydrolysis over a period of ≥2 h; and (*iii*) DA-ZP1-TPP responds to changes in intracellular mobile zinc levels, an observation corroborated by sensor shutoff on the addition of a chelator. Taken together, these data strongly support acetylation of fluorescein-based zinc sensors as an effective strategy both to improve the dynamic range of fluorescein-based zinc sensors and to facilitate cellular targeting by a localization vector.

DA-ZP1-TPP is a valuable addition to the arsenal of targetable small-molecule zinc-selective fluorescent probes. Currently, the most widely applied sensor for zinc in mitochondria is RhodZin-3, AM (40) (*SI Appendix*, Table S5), which requires endogenous esterases to activate and has a weak zinc affinity ($K_{\text{d-Zn}}$ ~65 nM). This value is well above the current estimates for mitochondrial mobile zinc concentrations (17). We anticipate that this strategy will be applicable to related families of fluorophores as well.

Investigating Zinc Trafficking to Mitochondria in Prostate Cells. With a new mitochondrial-targeting sensor in hand, we used DA-ZP1-TPP to investigate the ability of prostate cell lines to accumulate zinc within their mitochondria. RWPE-1 and RWPE-2 are a pair of genetically similar cell lines that retain normal epithelial cell morphology, express cytokeratin markers for prostate epithelial cells, and are hormone-sensitive (49, 50). RWPE-2 cells are tumorigenic, however, and accumulate less zinc owing to decreased ZIP1 expression and altered cellular localization of ZIP3 (11, 50).

To explore the ability of RWPE-1 and RWPE-2 cells to sequester zinc in mitochondria, we measured the fluorescence intensity of DA-ZP1-TPP in both lines after the cells were bathed in normal or zinc-enriched (50 μM $ZnCl_2$) keratinocyte serum-free medium for 24 h before imaging. The fluorescence signal intensity was ~2.3-fold higher in RWPE-1 cells bathed in zinc-enriched medium compared with cells bathed in normal medium (Fig. 8 and *SI Appendix*, Fig. S18). This result is consistent with the ability of healthy epithelial prostate cells to accumulate high

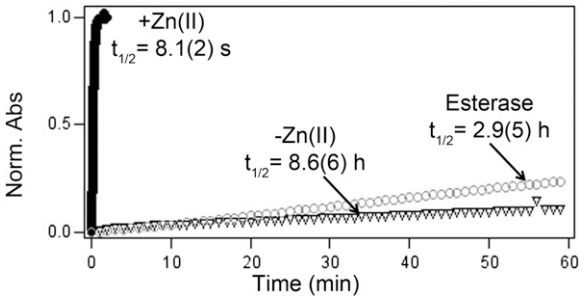

Fig. 6. Kinetic traces for the deacetylation of DA-ZP1-TPP. The half-life for deacetylation of a 2.75 μM solution of DA-ZP1-TPP at 37 °C in buffer (50 mM PIPES, 100 mM KCl; pH 7), was measured in the presence of 125 μM $ZnCl_2$ (black circles), 250 μM EDTA (triangle), or 1.25 U of porcine liver esterase (white circles). The change in absorbance at 520 nm (EDTA and esterase) or 510 nm ($ZnCl_2$) was used to monitor the reaction.

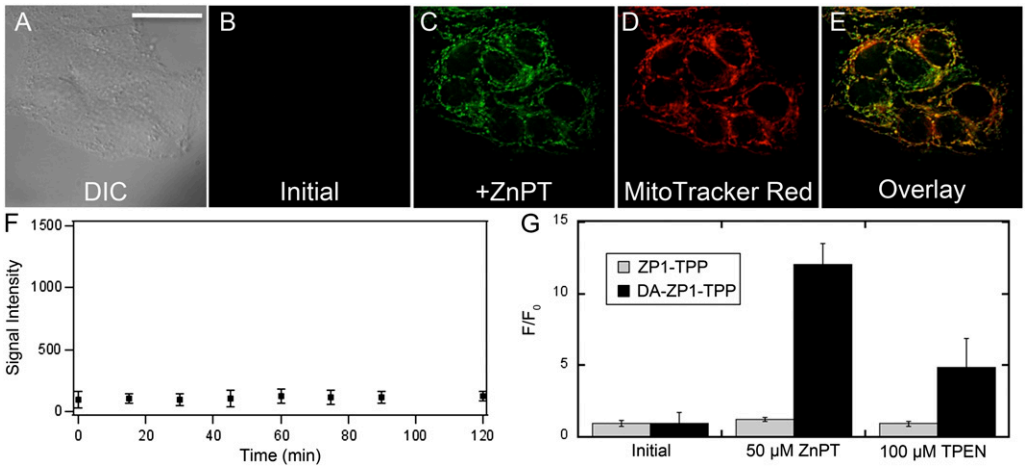

Fig. 7. Fluorescence imaging of live HeLa cells. (*A*) DIC image. (*B*) Initial fluorescence image, showing a minimal fluorescence signal, which was stable for a period of 2 h (*F*). (*C*) Addition of 50 μM ZnPT. (*D*) Signal from MitoTracker Red. (*E*) Overlay of *C* and *D*. Pearson's $r = 0.64 \pm 0.1$ ($n = 18$). (*G*) Quantification of the change in fluorescence signal intensity of DA-ZP1-TPP (black bars) compared with ZP1-TPP (gray bars) under similar conditions. (Scale bar: 37 μm.)

concentrations of total zinc (50, 51), but it also reveals that the observed changes correlate with increased mobile zinc within mitochondria. In contrast, RWPE-2 cells showed no statistically significant increase in fluorescence signal under analogous conditions (Fig. 8). Importantly, in both cell lines, the observed fluorescence signals from DA-ZP1-TPP are sensitive to TPEN and ZnPT and have good correlation with MitoTracker Red [$r = 0.68 \pm 0.09$ for RWPE-1 and 0.59 ± 0.1 for RWPE-2 (*SI Appendix*, Figs. S16–S18].

To further corroborate these observations, we conducted an analogous experiment in PC-3 cells, a model cell line for human prostatic adenocarcinoma metastatic to bone (52). In PC-3 cells, DA-ZP1-TPP correlated with MitoTracker Red qualitatively but with a lower correlation coefficient ($r = 0.32 \pm 0.1$) (*SI Appendix*, Fig. S19). Consistent with the results for the RWPE cell line, PC-3 cells showed no statistically significant increase in sensor fluorescence intensity when bathed in zinc-enriched (50 μM $ZnCl_2$) RMPI 1640 medium with 10% FBS for 24 h before imaging (Fig. 8).

To account for the zinc-binding ability of FBS (53), we repeated the imaging experiments with PC-3 cells in serum-free RMPI 1640 medium supplemented with 15 μM $ZnCl_2$ for 3 h (*SI Appendix*, Fig. S20) (54). Under these conditions, no statistically significant increase in fluorescence intensity was observed.

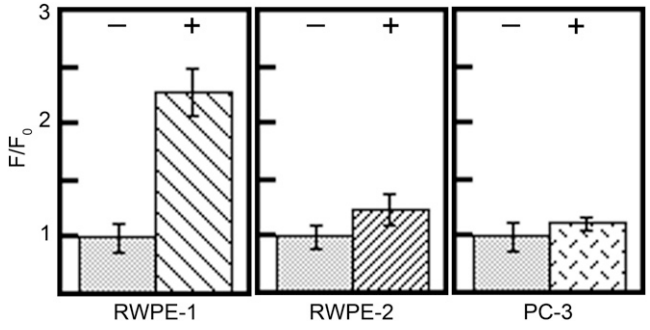

Fig. 8. Decreased mitochondrial zinc uptake in cancerous cell lines. RWPE-1, RWPE-2, and PC-3 prostate cell lines were incubated for 24 h in medium supplemented with (+) and without (–) 50 μM $ZnCl_2$. RWPE-1 is the only cell line demonstrating a statistically significant ($P < 0.001$) increase in mitochondrial zinc uptake when incubated in zinc-enriched media.

Our fluorescence imaging results from the RWPE and PC-3 cell lines are in agreement with the results of studies using homogenized prostatic tissue, which assert a correlation between altered zinc trafficking and prostate cancer (8, 11–13). These data demonstrate the inability of tumorigenic prostate cells to accumulate mobile zinc within their mitochondria. The inability of cancer cells to accumulate mobile zinc within mitochondria is consistent with the theory that tumors need an active mitochondrial aconitase to meet the energy demands of rapidly dividing cells (6). However, the RWPE-1, RWPE-2 (*SI Appendix*, Fig. S21), and PC-3 cell lines all accumulate increased levels of total zinc when bathed in zinc-enriched medium (9, 11, 50).

The ability of cancer cells to accumulate zinc, along with with the lack of a defined mitochondrial zinc transporter (7), raise questions about the mechanism of mobile zinc accumulation within mitochondria of prostatic epithelial cells, and how zinc trafficking is altered in tumorigenic cells. One possible explanation is differential expression of metallothionein isoforms in cancer cell lines (54); another is altered zinc trafficking pathways resulting from modified signaling cascades and transcription factor activity (13, 55, 56). Addressing these and other possibilities will require a detailed molecular understanding of the action of mobile zinc within healthy and tumorigenic prostate cells. In combination with biochemical investigations, the ability to direct zinc-responsive fluorescent probes to discrete cellular locales should provide valuable insight into the function of mobile zinc within the prostate.

Conclusion

DA-ZP1-TPP is a zinc-selective, reaction-based, fluorescent sensor that has an excellent dynamic range and pH profile, and it can be targeted to mitochondria in live cells. Acetylation of fluorescein-based zinc sensors simultaneously increases hydrophobicity and reduces the anionic character of the constructs, which in turn improves the cellular uptake and targetability of the probes. In contrast to the nonacetylated derivative, DA-ZP1-TPP has a vastly improved dynamic range and pH profile, and it can target mitochondria in live cells. DA-ZP1-TPP imaging of epithelial prostate cells revealed that tumorigenic lines lose the ability to accumulate mobile zinc within their mitochondria. Understanding mobile zinc trafficking in biology will require reagents such as DA-ZP1-TPP, which have the ability to visualize changes in free Zn^{2+} concentrations at discrete cellular locales. By creating a mobile zinc map and tracking the accumulation and fluctuation of

mobile zinc concentrations within the cell, we can begin to decipher the spatiotemporal mechanism behind the actions of mobile zinc and improve our understanding of its biology.

Materials and Methods

Materials and procedures for all experiments are supplied in the *SI Appendix*. Included in this appendix are the synthesis and characterization of compounds, mammalian cell culturing procedures, and details regarding fluorescence microscopy experiments. Also provided are additional figures, tables, and schemes relating to the characterization of compounds.

ACKNOWLEDGMENTS. We thank Dr. Ying Song for the (2-aminoethyl) triphenylphosphonium bromide and Dr. Zhen Huang and Ali Liang for helpful discussions. This work was funded by a grant from the National Institute of General Medical Sciences (GM065519, to S.J.L.). W.C. and D.Y.Z. would also like to thank Massachusetts Institute of Technology's Undergraduate Research Opportunities Program for funding.

1. Bertini I, Gray HB, Stiefel EI, Valentine JS (2007) *Biological Inorganic Chemistry: Structure and Reactivity* (University Science Books, Sausalito, CA).
2. Costello LC, Fenselau CC, Franklin RB (2011) Evidence for Operation of the Direct Zinc Ligand Exchange Mechanism for Trafficking, Transport, and Reactivity of Zinc in Mammalian Cells. *J Inorg Biochem* 105(5):589–599.
3. Pluth MD, Tomat E, Lippard SJ (2011) Biochemistry of mobile zinc and nitric oxide revealed by fluorescent sensors. *Annu Rev Biochem* 80:333–355.
4. Gundelfinger ED, Boeckers TM, Baron MK, Bowie JU (2006) A role for zinc in post-synaptic density asSAMbly and plasticity? *Trends Biochem Sci* 31(7):366–373.
5. Sensi SL, et al. (2011) The neurophysiology and pathology of brain zinc. *J Neurosci* 31(45):16076–16085.
6. Costello LC, Franklin RB, Feng P (2005) Mitochondrial function, zinc, and intermediary metabolism relationships in normal prostate and prostate cancer. *Mitochondrion* 5(3): 143–153.
7. Kelleher SL, McCormick NH, Velasquez V, Lopez V (2011) Zinc in specialized secretory tissues: Roles in the pancreas, prostate, and mammary gland. *Adv Nutr* 2(2):101–111.
8. Costello LC, Franklin RB (2011) Zinc is decreased in prostate cancer: An established relationship of prostate cancer! *J Biol Inorg Chem* 16(1):3–8.
9. Franklin RB, et al. (2003) Human ZIP1 is a major zinc uptake transporter for the accumulation of zinc in prostate cells. *J Inorg Biochem* 96(2-3):435–442.
10. Costello LC, Franklin RB, Liu Y, Kennedy MC (2000) Zinc causes a shift toward citrate at equilibrium of the m-aconitase reaction of prostate mitochondria. *J Inorg Biochem* 78(2):161–165.
11. Ghosh SK, et al. (2010) A novel imaging approach for early detection of prostate cancer based on endogenous zinc sensing. *Cancer Res* 70(15):6119–6127.
12. Tepaamorndech S, Huang L, Kirschke CP (2011) A null-mutation in the Znt7 gene accelerates prostate tumor formation in a transgenic adenocarcinoma mouse prostate model. *Cancer Lett* 308(1):33–42.
13. Kolenko V, Teper E, Kutikov A, Uzzo R (2013) Zinc and zinc transporters in prostate carcinogenesis. *Nat Rev Urol* 10(4):219–226.
14. Dean KM, Qin Y, Palmer AE (2012) Visualizing metal ions in cells: An overview of analytical techniques, approaches, and probes. *Biochim Biophys Acta* 1823(9):1406–1415.
15. Que EL, Domaille DW, Chang CJ (2008) Metals in neurobiology: Probing their chemistry and biology with molecular imaging. *Chem Rev* 108(5):1517–1549.
16. Nolan EM, Lippard SJ (2009) Small-molecule fluorescent sensors for investigating zinc metalloneurochemistry. *Acc Chem Res* 42(1):193–203.
17. Park JG, Qin Y, Galati DF, Palmer AE (2012) New sensors for quantitative measurement of mitochondrial Zn^{2+}. *ACS Chem Biol* 7(10):1636–1640.
18. McCranor BJ, et al. (2012) Quantitative imaging of mitochondrial and cytosolic free zinc levels in an in vitro model of ischemia/reperfusion. *J Bioenerg Biomembr* 44(2): 253–263.
19. Tomat E, Nolan EM, Jaworski J, Lippard SJ (2008) Organelle-specific zinc detection using Zinpyr-labeled fusion proteins in live cells. *J Am Chem Soc* 130(47):15776–15777.
20. Radford RJ, Chyan W, Lippard SJ (2013) Peptide-based targeting of fluorescent zinc sensors to the plasma membrane of live cells. *Chem Sci* 4(8):3080–3084.
21. Lim CS, et al. (2011) Ratiometric detection of mitochondrial thiols with a two-photon fluorescent probe. *J Am Chem Soc* 133(29):11132–11135.
22. Dodani SC, Leary SC, Cobine PA, Winge DR, Chang CJ (2011) A targetable fluorescent sensor reveals that copper-deficient *SCO1* and *SCO2* patient cells prioritize mitochondrial copper homeostasis. *J Am Chem Soc* 133(22):8606–8616.
23. Dickinson BC, Chang CJ (2008) A targetable fluorescent probe for imaging hydrogen peroxide in the mitochondria of living cells. *J Am Chem Soc* 130(30):9638–9639.
24. Masanta G, et al. (2011) A mitochondrial-targeted two-photon probe for zinc ion. *J Am Chem Soc* 133(15):5698–5700.
25. Sreenath K, Allen JR, Davidson MW, Zhu L (2011) A FRET-based indicator for imaging mitochondrial zinc ions. *Chem Commun (Camb)* 47(42):11730–11732.
26. Liu Z, Zhang C, Chen Y, He W, Guo Z (2012) An excitation ratiometric Zn^{2+} sensor with mitochondria-targetability for monitoring of mitochondrial Zn^{2+} release upon different stimulations. *Chem Commun (Camb)* 48(67):8365–8367.
27. Baek NY, et al. (2012) A highly sensitive two-photon fluorescent probe for mitochondrial zinc ions in living tissue. *Chem Commun (Camb)* 48(38):4546–4548.
28. Aoki S, et al. (2008) Design and synthesis of a caged Zn^{2+} probe, 8-benzenesulfonyloxy-5-*N,N*-dimethylaminosulfonylquinolin-2-ylmethyl-pendant 1,4,7,10-tetraazacyclododecane, and its hydrolytic uncaging upon complexation with Zn^{2+}. *Inorg Chem* 47(7):2747–2754.
29. Jun ME, Roy B, Ahn KH (2011) "Turn-on" fluorescent sensing with "reactive" probes. *Chem Commun (Camb)* 47(27):7583–7601.
30. Chan J, Dodani SC, Chang CJ (2012) Reaction-based small-molecule fluorescent probes for chemoselective bioimaging. *Nat Chem* 4(12):973–984.
31. Maryanoff BE, Reitz AB, Duhl-Emswiler BA (1985) Stereochemistry of the Wittig reaction: Effect of nucleophilic groups in the phosphonium ylide. *J Am Chem Soc* 107(1): 217–226.
32. Smith RAJ, Porteous CM, Gane AM, Murphy MP (2003) Delivery of bioactive molecules to mitochondria in vivo. *Proc Natl Acad Sci USA* 100(9):5407–5412.
33. Woodroofe CC, Masalha R, Barnes KR, Frederickson CJ, Lippard SJ (2004) Membrane-permeable and -impermeable sensors of the Zinpyr family and their application to imaging of hippocampal zinc in vivo. *Chem Biol* 11(12):1659–1666.
34. Wong BA, Friedle S, Lippard SJ (2009) Solution and fluorescence properties of symmetric dipicolylamine-containing dichlorofluorescein-based Zn^{2+} sensors. *J Am Chem Soc* 131(20):7142–7152.
35. Neto BAD, Corrêa JR, Silva RG (2013) Selective mitochondrial staining with small fluorescent probes: Importance, design, synthesis, challenges and trends for new markers. *RSC Adv.* 3(16):5291–5301.
36. Yousif LF, Stewart KM, Kelley SO (2009) Targeting mitochondria with organelle-specific compounds: Strategies and applications. *ChemBioChem* 10(12):1939–1950.
37. Jiang PJ, Guo ZJ (2004) Fluorescent detection of zinc in biological systems: Recent development on the design of chemosensors and biosensors. *Coord Chem Rev* 248(1-2): 205–229.
38. Izumi S, Urano Y, Hanaoka K, Terai T, Nagano T (2009) A simple and effective strategy to increase the sensitivity of fluorescence probes in living cells. *J Am Chem Soc* 131(29):10189–10200.
39. Lavis LD, Chao TY, Raines RT (2011) Synthesis and utility of fluorogenic acetoxymethyl ethers. *Chem Sci* 2(3):521–530.
40. Johnson I, Spence MTZ (2010) *Molecular Probes Handbook: A Guide to Fluorescent Probes and Labeling Technology* (Life Technologies, Carlsbad, CA), 11th Ed.
41. Takahashi A, Camacho P, Lechleiter JD, Herman B (1999) Measurement of intracellular calcium. *Physiol Rev* 79(4):1089–1125.
42. Hegg EL, Burstyn JN (1998) Toward the development of metal-based synthetic nucleases and peptidases: A rationale and progress report in applying the principles of coordination chemistry. *Coord Chem Rev* 173:133–165.
43. Walkup GK, Burdette SC, Lippard SJ, Tsien RY (2000) A new cell-permeable fluorescent probe for Zn^{2+}. *J Am Chem Soc* 122(23):5644–5645.
44. Finney LA, O'Halloran TV (2003) Transition metal speciation in the cell: Insights from the chemistry of metal ion receptors. *Science* 300(5621):931–936.
45. Nolan EM, et al. (2005) QZ1 and QZ2: Rapid, reversible quinoline-derivatized fluoresceins for sensing biological Zn(II). *J Am Chem Soc* 127(48):16812–16823.
46. Mancin F, Scrimin P, Tecilla P (2012) Progress in artificial metallonucleases. *Chem Commun (Camb)* 48(45):5545–5559.
47. Au-Yeung HY, New EJ, Chang CJ (2012) A selective reaction-based fluorescent probe for detecting cobalt in living cells. *Chem Commun (Camb)* 48(43):5268–5270.
48. Kierat RM, Krämer R (2005) A fluorogenic and chromogenic probe that detects the esterase activity of trace copper(II). *Bioorg Med Chem Lett* 15(21):4824–4827.
49. Bello D, Webber MM, Kleinman HK, Wartinger DD, Rhim JS (1997) Androgen responsive adult human prostatic epithelial cell lines immortalized by human papillomavirus 18. *Carcinogenesis* 18(6):1215–1223.
50. Huang L, Kirschke CP, Zhang Y (2006) Decreased intracellular zinc in human tumorigenic prostate epithelial cells: A possible role in prostate cancer progression. *Cancer Cell Int* 6:10.
51. Liu Y, Franklin RB, Costello LC (1997) Prolactin and testosterone regulation of mitochondrial zinc in prostate epithelial cells. *Prostate* 30(1):26–32.
52. Kaighn ME, Narayan KS, Ohnuki Y, Lechner JF, Jones LW (1979) Establishment and characterization of a human prostatic carcinoma cell line (PC-3). *Invest Urol* 17(1): 16–23.
53. Bozym RA, et al. (2010) Free zinc ions outside a narrow concentration range are toxic to a variety of cells in vitro. *Exp Biol Med (Maywood)* 235(6):741–750.
54. Wei H, et al. (2008) Differential expression of metallothioneins (MTs) 1, 2, and 3 in response to zinc treatment in human prostate normal and malignant cells and tissues. *Mol Cancer* 7:7.
55. Golovine K, et al. (2008) Overexpression of the zinc uptake transporter hZIP1 inhibits nuclear factor-kappaB and reduces the malignant potential of prostate cancer cells in vitro and in vivo. *Clin Cancer Res* 14(17):5376–5384.
56. Carraway RE, Dobner PR (2012) Zinc pyrithione induces ERK- and PKC-dependent necrosis distinct from TPEN-induced apoptosis in prostate cancer cells. *Biochim Biophys Acta* 1823(2):544–557.